Substructure Stiffness and Mass Updating through Minimization of Modal Dynamic Residuals

Dapeng Zhu, Xinjun Dong, Yang Wang*

School of Civil and Environmental Engineering, Georgia Institute of Technology, Atlanta, GA, USA

ABSTRACT

This research studies a substructure finite element model updating approach that requires vibration data from only part of a large structure (i.e. a substructure). Craig-Bampton transform is adopted to condense the residual structure using a limited number of dominant modal coordinates, while the substructure model remains at high resolution. To update the condensed model, physical parameters in the substructure and modal parameters of the residual structure are chosen as optimization variables; minimization of modal dynamic residuals from the eigenvalue equations in structural dynamics is chosen as the optimization objective. An iterative linearization procedure is adopted for efficiently solving the optimization problem. The proposed substructure model updating approach is validated with 1D, 2D and 3D examples.

Keywords: finite element model updating, substructure modeling, modal dynamic residual, iterative linearization

INTRODUCTION

In order to simulate structural behavior under various loading conditions, finite element (FE) models are often constructed. However, predictions by FE models often differ from experimental results at the actual structure. The discrepancies are mainly caused by inaccuracies in FE models. For example, simplifications are usually adopted in FE modeling, such as idealized hinges and rollers, whereas the simplified conditions do not exist in reality. In addition, FE models often adopt nominal material properties, while the actual properties may be

Dapeng Zhu is with the School of Civil and Environmental Engineering, Georgia Institute of Technology, Atlanta, GA
Xinjun Dong is with the School of Civil and Environmental Engineering, Georgia Institute of Technology, Atlanta, GA
Yang Wang* is with the School of Civil and Environmental Engineering, Georgia Institute of Technology, Atlanta, GA
(email : yang.wang@ce.gatech.edu; phone: +1(404) 894-1851; fax: +1(404)385-0337))

different in the field. Therefore, for higher simulation accuracy, experimental data collected from the actual structure in the field can be used to update the FE model parameters, which is known as model updating.

Many FE model updating algorithms have been developed and practically applied in the past few decades (Friswell and Mottershead 1995). Most algorithms can be categorized into two groups, i.e. frequency-domain approaches and time-domain approaches. Frequency-domain approaches update an FE model using vibration modal properties extracted from experimental measurement (such as natural frequencies, mode shapes, and damping ratios) (Farhat and Hemez 1993; Sanayei *et al.* 1999; Sanayei *et al.* 2001; Jaishi and Ren 2006). Compared to frequency-domain approaches, time-domain approaches deal with time history data directly, without the requirement for extracting modal properties (Hoshiya and Saito 1984; Loh and Tou 1995; Smyth *et al.* 1999; Smyth *et al.* 2002; Yang and Huang 2007a; Yang *et al.* 2007). When applied to a high-resolution FE model of a large structure, many existing approaches suffer computational and convergence difficulties. The reason is that both approaches operate on a complete FE model for the entire structure, which usually contains a very large number of degrees of freedom (DOFs).

In order to alleviate the computational difficulty, particularly to accommodate data collected at dense measurement locations on large structures, substructure-based FE model updating can be pursued. Research activities have been reported on substructure model updating in both frequency domain and time domain. As an example of frequency domain approaches, Link adopted Craig-Bampton transform for substructure modeling, and updated the substructure model by minimizing difference between simulated and experimental modal properties (Craig and Bampton 1968; Link 1998; Craig 2000). Other studies used frequency spectra for substructure model updating, by minimizing difference between simulated and experimental spectra in certain frequency range (Zhao *et al.* 1995; Zhang and Johnson 2013a; Zhang and Johnson 2013b). In (Koh and Shankar 2003), the interface force vector was estimated using multiple sets of measurement; the difference between multiple estimations was minimized with genetic algorithms for substructure model updating. Among time-domain approaches, researchers applied the extended Kalman filter approach for substructure model updating

of a simulated shear building model (Koh *et al.* 1991; Trinh and Koh 2012). A "quasi-static displacement" concept has been proposed for substructure formulation, so that only the acceleration time histories of the interface DOFs were required (Koh *et al.* 2003). Recently, a substructure model updating procedure is proposed using Bayes' theorem, without requiring interface measurements or excitation measurements (Yuen and Katafygiotis 2006). In addition, the sequential nonlinear least square estimation (SNLSE) method has been investigated for substructure model updating (Yang and Huang 2007b); the unknown interface coupling terms were treated as unknown forces, and sequentially updated in each time step with state variables and system parameters. Finally, a substructure isolation approach is developed based on virtual distortion method; the approach was validated numerically with a plane frame, and experimentally with a continuous beam (Hou *et al.* 2011).

Overall, most of the existing substructure model updating approaches have only been validated with simplistic structural models, where 1D lumped spring-mass models are the most common. Many approaches are reported with convergence problems, either due to a bad initial guess of structural parameters or the high nonlinearity of the objective functions. This research investigates substructure updating using frequency domain data. To reduce computational difficulty, the entire structural model is divided into a substructure (currently being instrumented and to be updated) and the residual structure. Craig-Bampton transform is adopted to condense the residual structure using a limited number of dominant modal coordinates, while the substructure model remains at high resolution. To update the condensed model, physical parameters in the substructure and modal parameters of the residual structure are chosen as optimization variables; minimization of the modal dynamic residuals from the eigenvalue equations in structural dynamics is chosen as the optimization objective. An iterative linearization procedure is adopted for efficiently solving the optimization problem (Farhat and Hemez 1993; Zhu and Wang 2012; Zhu *et al.* 2013).

The rest of the paper is organized as follows. Section 2 presents the formulation of substructure modeling. Section 3 describes substructure updating through the optimization procedure of iteratively minimizing modal

dynamic residuals. Section 4 shows three numerical examples (ranging from 1D to 3D) for validating the proposed approach. The performance of the proposed approach is compared with a conventional updating procedure that minimizes experimental and simulated modal property difference. Finally, a summary and discussion are provided.

SUBSTRUCTURE MODELING

This section presents the basic formulation for substructure modeling. The first subsection describes the model condensation strategy following Craig-Bampton transform. The second subsection describes the formulations of sensitivity matrices for model updating variables.

Substructure Model Condensation

Figure 1 illustrates the substructure modeling strategy following (Craig and Bampton 1968; Craig 2000) . Subscripts S, I, and R are used to denote DOFs associated with the substructure being analyzed, the interface nodes, and the residual structure, respectively. The block-bidiagonal structural stiffness and mass matrices, $\mathbf{K}$ and $\mathbf{M} \in \mathbb{R}^{n_S+n_I+n_R}$, can be assembled using original DOFs $\mathbf{x} = \begin{bmatrix} \mathbf{x}_S & \mathbf{x}_I & \mathbf{x}_R \end{bmatrix}^T$.

$$\mathbf{K} = \begin{bmatrix} \begin{bmatrix} \mathbf{K}_S \end{bmatrix} & \mathbf{0} \\ \mathbf{0} & \mathbf{0} \end{bmatrix} + \begin{bmatrix} \mathbf{0} & \mathbf{0} & \mathbf{0} \\ \mathbf{0} & \begin{bmatrix} \mathbf{K}_R \end{bmatrix} \end{bmatrix} = \begin{bmatrix} \begin{bmatrix} \mathbf{K}_{SS} & \mathbf{K}_{SI} \\ \mathbf{K}_{IS} & \mathbf{K}_{II}^S \end{bmatrix} & \mathbf{0} \\ \mathbf{0} & \mathbf{0} \end{bmatrix} + \begin{bmatrix} \mathbf{0} & \mathbf{0} & \mathbf{0} \\ \mathbf{0} & \begin{bmatrix} \mathbf{K}_{II}^R & \mathbf{K}_{IR} \\ \mathbf{K}_{RI} & \mathbf{K}_{RR} \end{bmatrix} \end{bmatrix} \tag{1}$$

$$\mathbf{M} = \begin{bmatrix} \begin{bmatrix} \mathbf{M}_S \end{bmatrix} & \mathbf{0} \\ \mathbf{0} & \mathbf{0} \end{bmatrix} + \begin{bmatrix} \mathbf{0} & \mathbf{0} & \mathbf{0} \\ \mathbf{0} & \begin{bmatrix} \mathbf{M}_R \end{bmatrix} \end{bmatrix} = \begin{bmatrix} \begin{bmatrix} \mathbf{M}_{SS} & \mathbf{M}_{SI} \\ \mathbf{M}_{IS} & \mathbf{M}_{II}^S \end{bmatrix} & \mathbf{0} \\ \mathbf{0} & \mathbf{0} \end{bmatrix} + \begin{bmatrix} \mathbf{0} & \mathbf{0} & \mathbf{0} \\ \mathbf{0} & \begin{bmatrix} \mathbf{M}_{II}^R & \mathbf{M}_{IR} \\ \mathbf{M}_{RI} & \mathbf{M}_{RR} \end{bmatrix} \end{bmatrix} \tag{2}$$

Here $\mathbf{K}_S$ and $\mathbf{M}_S$ denote entries of the stiffness and mass matrices corresponding to the substructure; $\mathbf{K}_R$ and $\mathbf{M}_R$ denote entries corresponding to the residual structure; $\mathbf{K}_{II}^S$ and $\mathbf{M}_{II}^S$ denote the entries at the interface DOFs and contributed by members of the substructure; $\mathbf{K}_{II}^R$ and $\mathbf{M}_{II}^R$ denote entries at the interface DOFs and contributed by members of the residual structure.

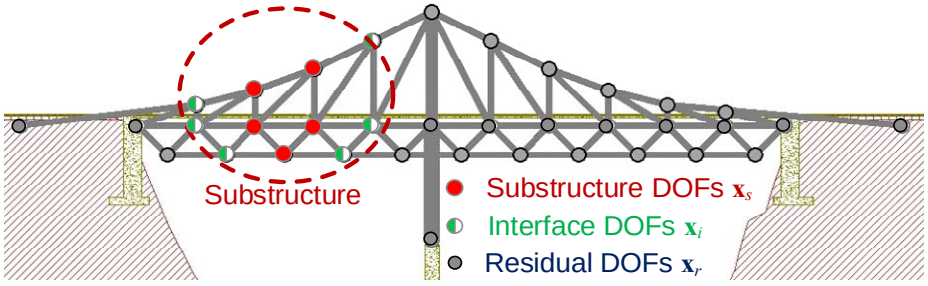

Figure 1. Illustration of substructure modeling strategy

Dynamic behavior of the residual structure can be approximated using Craig-Bampton transform (Craig and Bampton 1968; Craig 2000). The DOFs of the residual structure, $\mathbf{x}_\mathrm{R} \in \mathbb{R}^{n_\mathrm{R}}$, are approximated by a linear combination of interface DOFs, $\mathbf{x}_\mathrm{I} \in \mathbb{R}^{n_\mathrm{I}}$, and modal coordinates of the residual structure, $\mathbf{q}_\mathrm{R} \in \mathbb{R}^{n_q}$.

$$\mathbf{x}_\mathrm{R} \approx \mathbf{T}\mathbf{x}_\mathrm{I} + \mathbf{\Phi}_\mathrm{R}\mathbf{q}_\mathrm{R} \tag{3}$$

Here $\mathbf{T} = -\mathbf{K}_{\mathrm{RR}}^{-1}\mathbf{K}_{\mathrm{RI}} \in \mathbb{R}^{n_\mathrm{R} \times n_\mathrm{I}}$ is the Guyan static condensation matrix; $\mathbf{\Phi}_\mathrm{R} = \left[\boldsymbol{\varphi}_1, \ldots, \boldsymbol{\varphi}_{n_q}\right] \in \mathbb{R}^{n_\mathrm{R} \times n_q}$ represents the mode shapes of the residual structure with interface DOFs fixed. Although the size of the residual structure may be large, the number of modal coordinates, n_q, can be chosen as relatively small to reflect the first few dominant mode shapes only (i.e. $n_q << n_\mathrm{R}$). The coordinate transformation is rewritten in vector form as:

$$\begin{bmatrix} \mathbf{x}_\mathrm{I} \\ \mathbf{x}_\mathrm{R} \end{bmatrix} \approx \mathbf{\Gamma} \begin{bmatrix} \mathbf{x}_\mathrm{I} \\ \mathbf{q}_\mathrm{R} \end{bmatrix}, \text{ where } \mathbf{\Gamma} = \begin{bmatrix} \mathbf{I} & \\ \mathbf{T} & \mathbf{\Phi}_\mathrm{R} \end{bmatrix} \tag{4}$$

Suppose $\tilde{\mathbf{K}}_\mathrm{R}$ and $\tilde{\mathbf{M}}_\mathrm{R} \in \mathbb{R}^{(n_\mathrm{I}+n_\mathrm{q}) \times (n_\mathrm{I}+n_\mathrm{q})}$ denote the new stiffness and mass matrices of the residual structure after transformation:

$$\tilde{\mathbf{K}}_\mathrm{R} = \mathbf{\Gamma}^\mathrm{T}\mathbf{K}_\mathrm{R}\mathbf{\Gamma} = \begin{bmatrix} \tilde{\mathbf{K}}_{\mathrm{II}} & \\ & \boldsymbol{\gamma} \end{bmatrix} = \begin{bmatrix} \mathbf{K}_{\mathrm{II}}^\mathrm{R} + \mathbf{T}^\mathrm{T}\mathbf{K}_{\mathrm{RI}} & \\ & \mathbf{\Phi}_\mathrm{R}^\mathrm{T}\mathbf{K}_{\mathrm{RR}}\mathbf{\Phi}_\mathrm{R} \end{bmatrix} \tag{5}$$

$$\tilde{\mathbf{M}}_\mathrm{R} = \mathbf{\Gamma}^\mathrm{T}\mathbf{M}_\mathrm{R}\mathbf{\Gamma} = \begin{bmatrix} \tilde{\mathbf{M}}_{\mathrm{II}} & \tilde{\mathbf{M}}_{\mathrm{I}q} \\ \tilde{\mathbf{M}}_{q\mathrm{I}} & \boldsymbol{\mu} \end{bmatrix} = \begin{bmatrix} \mathbf{M}_{\mathrm{II}}^\mathrm{R} + \mathbf{T}^\mathrm{T}\mathbf{M}_{\mathrm{RI}} + \mathbf{M}_{\mathrm{IR}}\mathbf{T} + \mathbf{T}^\mathrm{T}\mathbf{M}_{\mathrm{RR}}\mathbf{T} & (\mathbf{M}_{\mathrm{IR}} + \mathbf{T}^\mathrm{T}\mathbf{M}_{\mathrm{RR}})\mathbf{\Phi}_\mathrm{R} \\ \mathbf{\Phi}_\mathrm{R}^\mathrm{T}(\mathbf{M}_{\mathrm{RI}} + \mathbf{M}_{\mathrm{RR}}\mathbf{T}) & \mathbf{\Phi}_\mathrm{R}^\mathrm{T}\mathbf{M}_{\mathrm{RR}}\mathbf{\Phi}_\mathrm{R} \end{bmatrix} \tag{6}$$

where $\boldsymbol{\gamma} = \text{diag}(\gamma_1, \cdots, \gamma_{n_q})$ and $\boldsymbol{\mu} = \text{diag}(\mu_1, \cdots, \mu_{n_q})$ are diagonal modal stiffness and modal mass matrices of the residual structure fixed at the interface. Note that due to the static condensation process in this transformation, the off-diagonal block entries of $\tilde{\mathbf{K}}_{\text{R}}$ are zero.

Upon transformation to the residual structure, a new set of stiffness matrix $\tilde{\mathbf{K}}$ and structural mass matrix $\tilde{\mathbf{M}}$ of the entire structure can be assembled. In this assembly, contribution from the substructure, $\mathbf{K}_{\text{S}}$ and $\mathbf{M}_{\text{S}}$ (Equations (1) and (2)), remains unchanged. In other words, the substructure model remains at original high resolution, in order to enable accurate updating of substructure parameters. Because only a few dominant modal coordinates of the residual structure are adopted (i.e. $n_q << n_{\text{R}}$), dimension of $\tilde{\mathbf{K}}$ and $\tilde{\mathbf{M}}$ (both are $n_{\text{S}} + n_{\text{I}} + n_q$) is condensed to be much smaller than original matrices $\mathbf{K}$ and $\mathbf{M}$ ($n_{\text{S}} + n_{\text{I}} + n_{\text{R}}$).

$$\tilde{\mathbf{K}} = \begin{bmatrix} \begin{bmatrix} \mathbf{K}_{\text{S}} \end{bmatrix} & \mathbf{0} \\ \mathbf{0} \quad \mathbf{0} & \mathbf{0} \end{bmatrix} + \begin{bmatrix} \mathbf{0} & \mathbf{0} \quad \mathbf{0} \\ \mathbf{0} & \begin{bmatrix} \tilde{\mathbf{K}}_{\text{R}} \end{bmatrix} \\ \mathbf{0} & \end{bmatrix} \tag{7}$$

$$\tilde{\mathbf{M}} = \begin{bmatrix} \begin{bmatrix} \mathbf{M}_{\text{S}} \end{bmatrix} & \mathbf{0} \\ \mathbf{0} \quad \mathbf{0} & \mathbf{0} \end{bmatrix} + \begin{bmatrix} \mathbf{0} & \mathbf{0} \quad \mathbf{0} \\ \mathbf{0} & \begin{bmatrix} \tilde{\mathbf{M}}_{\text{R}} \end{bmatrix} \\ \mathbf{0} & \end{bmatrix} \tag{8}$$

Sensitivity of Updating Variables

The updating variable for the substructure are physical parameters, e.g. elastic modulus and density of each substructure element. When the updating parameters are independent, the substructure matrices can be updated as functions of updating variables $\boldsymbol{\alpha} \in \mathbb{R}^{n_\alpha \times 1}$ and $\boldsymbol{\beta} \in \mathbb{R}^{n_\beta \times 1}$.

$$\mathbf{K}_{\text{S}}(\boldsymbol{\alpha}) = \mathbf{K}_{\text{S0}} + \sum_{j=1}^{n_\alpha} \alpha_j \mathbf{K}_{\text{S0},j} \qquad \mathbf{M}_{\text{S}}(\boldsymbol{\beta}) = \mathbf{M}_{\text{S0}} + \sum_{j=1}^{n_\beta} \beta_j \mathbf{M}_{\text{S0},j} \tag{9}$$

where $\mathbf{K}_{\text{S0}}$ and $\mathbf{M}_{\text{S0}}$ are the stiffness and mass matrices of the substructure and used as initial starting point in the model updating; α_j and β_j correspond to physical system parameters in the substructure to be updated; n_α and n_β represent the total number of corresponding parameters to be updated; $\mathbf{K}_{\text{S0},j}$ and $\mathbf{M}_{\text{S0},j}$ are constant

matrices determined by the type and location of these parameters. Subscript "0" will be used hereinafter to denote variables associated with the initial structural model, which serves as the starting point for model updating. For example, while $\mathbf{M}_{\mathrm{S}}(\boldsymbol{\beta})$ contains the aggregated contribution of all structural members, each $\mathbf{M}_{\mathrm{S0},j}$ corresponds to the contribution of one mass parameter. Although $\mathbf{M}_{\mathrm{S0}}$ may be assembled with initial/nominal parameter values that are less accurate, it should still contain contribution from all members and have the similar pattern as $\mathbf{M}_{\mathrm{S}}(\boldsymbol{\beta})$.

Link described a model updating method for the condensed residual structure matrices (Link 1998). The matrices of the condensed residual structural model, $\tilde{\mathbf{K}}_{\mathrm{R}}$ and $\tilde{\mathbf{M}}_{\mathrm{R}}$ in Equations (5) and (6), contains $(n_{\mathrm{I}} + n_q) \times (n_{\mathrm{I}} + n_q)$ number of entries. Assuming that physical changes in the original residual structure do not significantly alter the generalized eigenvectors of $\tilde{\mathbf{K}}_{\mathrm{R}}$ and $\tilde{\mathbf{M}}_{\mathrm{R}}$, only $(n_{\mathrm{I}} + n_q)$ number of modal parameters are selected as updating variables for each condensed matrix of the residual structural model. As a result, $\boldsymbol{\tau} \in \mathbb{R}^{(n_{\mathrm{I}}+n_q)\times 1}$ is the updating variable vector for $\tilde{\mathbf{K}}_{\mathrm{R}}$, and $\boldsymbol{\eta} \in \mathbb{R}^{(n_{\mathrm{I}}+n_q)\times 1}$ for $\tilde{\mathbf{M}}_{\mathrm{R}}$.

$$\tilde{\mathbf{K}}_{\mathrm{R}}(\boldsymbol{\tau}) = \tilde{\mathbf{K}}_{\mathrm{R0}} + \sum_{j=1}^{n_{\mathrm{I}}+n_q} \tau_j \tilde{\mathbf{K}}_{\mathrm{R0},j} \qquad \tilde{\mathbf{M}}_{\mathrm{R}}(\boldsymbol{\eta}) = \tilde{\mathbf{M}}_{\mathrm{R0}} + \sum_{j=1}^{n_{\mathrm{I}}+n_q} \eta_j \tilde{\mathbf{M}}_{\mathrm{R0},j} \tag{10}$$

where τ_j and η_j are the modal parameters to be updated; $\tilde{\mathbf{K}}_{\mathrm{R0}}$ and $\tilde{\mathbf{M}}_{\mathrm{R0}}$ are the initial stiffness and mass matrices of the condensed residual structure model; $\tilde{\mathbf{K}}_{\mathrm{R0},j}$ and $\tilde{\mathbf{M}}_{\mathrm{R0},j}$, each a rank-1 square matrix, represent the constant sensitivity matrices formulated using modal back-transform:

$$\tilde{\mathbf{K}}_{\mathrm{R0},j} = \boldsymbol{\varphi}^{l}_{\mathrm{R0},j} \omega^2_{\mathrm{R0},j} \boldsymbol{\varphi}^{l,\mathrm{T}}_{\mathrm{R0},j} \qquad \tilde{\mathbf{M}}_{\mathrm{R0},j} = \boldsymbol{\varphi}^{l}_{\mathrm{R0},j} \boldsymbol{\varphi}^{l,\mathrm{T}}_{\mathrm{R0},j} \tag{11}$$

where

$$\left[\boldsymbol{\varphi}^{l}_{\mathrm{R0},1} \quad \cdots \quad \boldsymbol{\varphi}^{l}_{\mathrm{R0},n_{\mathrm{I}}+n_q} \right] = \boldsymbol{\Phi}^{-\mathrm{T}}_{\mathrm{R0}} = \left[\boldsymbol{\varphi}_{\mathrm{R0},1} \quad \cdots \quad \boldsymbol{\varphi}_{\mathrm{R0},n_{\mathrm{I}}+n_q} \right]^{-\mathrm{T}} \tag{12}$$

$\omega^2_{\mathrm{R0},j}$ and $\boldsymbol{\varphi}_{\mathrm{R0},j}$ are the j-th generalized eigenvalue and mass-normalized eigenvector of the initial transformed residual structural model with free interface:

$$\boldsymbol{\Phi}_{\mathrm{R}0}^{\mathrm{T}}\tilde{\mathbf{M}}_{\mathrm{R}0}\boldsymbol{\Phi}_{\mathrm{R}0}=\mathbf{I}\qquad\boldsymbol{\Phi}_{\mathrm{R}0}^{\mathrm{T}}\tilde{\mathbf{K}}_{\mathrm{R}0}\boldsymbol{\Phi}_{\mathrm{R}0}=\mathrm{diag}(\omega_{\mathrm{R}0,1}^2,\cdots,\omega_{\mathrm{R}0,(n_q+n_\mathrm{I})}^2) \tag{13}$$

Using all model matrices to be updated, i.e. Equation (9) for substructure and Equation (10) for residual structure, the condensed entire structural model with reduced DOFs, $\begin{bmatrix}\mathbf{x}_\mathrm{S} & \mathbf{x}_\mathrm{I} & \mathbf{q}_\mathrm{R}\end{bmatrix}^\mathrm{T}$, can be updated with variables α_j, β_j, τ_j and η_j.

$$\begin{aligned}\tilde{\mathbf{K}}(\boldsymbol{\alpha},\boldsymbol{\tau})&=\begin{bmatrix}\begin{bmatrix}\mathbf{K}_\mathrm{S}\end{bmatrix} & \mathbf{0}\\ \mathbf{0} & \mathbf{0}\end{bmatrix}+\begin{bmatrix}\mathbf{0} & \mathbf{0} & \mathbf{0}\\ \mathbf{0} & \begin{bmatrix}\tilde{\mathbf{K}}_\mathrm{R}\end{bmatrix} & \\ \mathbf{0} & & \end{bmatrix}\\ &=\tilde{\mathbf{K}}_0+\sum_{j=1}^{n_\alpha}\alpha_j\begin{bmatrix}\begin{bmatrix}\mathbf{K}_{\mathrm{S}0,j}\end{bmatrix} & \mathbf{0}\\ \mathbf{0} & \mathbf{0}\end{bmatrix}+\sum_{j=1}^{n_\mathrm{I}+n_q}\tau_j\begin{bmatrix}\mathbf{0} & \mathbf{0} & \mathbf{0}\\ \mathbf{0} & \begin{bmatrix}\tilde{\mathbf{K}}_{\mathrm{R}0,j}\end{bmatrix} & \\ \mathbf{0} & & \end{bmatrix}\\ &=\tilde{\mathbf{K}}_0+\sum_{j=1}^{n_\alpha}\alpha_j\mathbf{S}_{\alpha,j}+\sum_{j=1}^{n_\mathrm{I}+n_q}\tau_j\mathbf{S}_{\tau,j}\end{aligned} \tag{14}$$

by defining

$$\tilde{\mathbf{K}}_0=\begin{bmatrix}\begin{bmatrix}\mathbf{K}_{\mathrm{S}0}\end{bmatrix} & \mathbf{0}\\ \mathbf{0} & \mathbf{0}\end{bmatrix}+\begin{bmatrix}\mathbf{0} & \mathbf{0} & \mathbf{0}\\ \mathbf{0} & \begin{bmatrix}\tilde{\mathbf{K}}_{\mathrm{R}0}\end{bmatrix} & \\ \mathbf{0} & & \end{bmatrix} \tag{15}$$

Similarly, the condensed mass matrix for the entire structure is written as:

$$\begin{aligned}\tilde{\mathbf{M}}(\boldsymbol{\beta},\boldsymbol{\eta})&=\tilde{\mathbf{M}}_0+\sum_{j=1}^{n_\beta}\beta_j\begin{bmatrix}\begin{bmatrix}\mathbf{M}_{\mathrm{S}0,j}\end{bmatrix} & \mathbf{0}\\ \mathbf{0} & \mathbf{0}\end{bmatrix}+\sum_{j=1}^{n_\mathrm{I}+n_q}\eta_j\begin{bmatrix}\mathbf{0} & \mathbf{0} & \mathbf{0}\\ \mathbf{0} & \begin{bmatrix}\tilde{\mathbf{M}}_{\mathrm{R}0,j}\end{bmatrix} & \\ \mathbf{0} & & \end{bmatrix}\\ &=\tilde{\mathbf{M}}_0+\sum_{j=1}^{n_\beta}\beta_j\mathbf{S}_{\beta,j}+\sum_{j=1}^{n_\mathrm{I}+n_q}\eta_j\mathbf{S}_{\eta,j}\end{aligned} \tag{16}$$

where $\mathbf{S}_{\alpha,j}$, $\mathbf{S}_{\beta,j}$, $\mathbf{S}_{\tau,j}$ and $\mathbf{S}_{\eta,j}$ represent the constant sensitivity matrices corresponding to variables α_j, β_j, τ_j and η_j, respectively.

SUBSTRUCTURE MODEL UPDATING

To update the condensed structural model, a modal dynamic residual approach is proposed in this study. For performance comparison, a conventional modal property difference approach is also considered in this study. In both approaches, it is assumed that sensors are deployed on the substructure and interface DOFs at high

density, so that mode shapes of the substructure can be identified from experimental data. Sensor instrumentation at the residual DOFs is not required. The first and second subsection describe the proposed modal dynamic residual approach and the conventional modal property difference approach, respectively.

Modal Dynamic Residual Approach

The proposed model updating approach attempts to minimize modal dynamic residuals of the generalized eigenvalue equation for the condensed structural model:

$$\begin{aligned} &\underset{\boldsymbol{\alpha},\boldsymbol{\beta},\boldsymbol{\tau},\boldsymbol{\eta},\boldsymbol{\psi}_{\mathrm{u}}}{\text{minimize}} \quad && \sum_{j=1}^{n_{\mathrm{m}}} \left\| \left[\tilde{\mathbf{K}}(\boldsymbol{\alpha},\boldsymbol{\tau}) - \omega_j^2 \tilde{\mathbf{M}}(\boldsymbol{\beta},\boldsymbol{\eta}) \right] \begin{Bmatrix} \boldsymbol{\psi}_{\mathrm{m},j} \\ \boldsymbol{\psi}_{\mathrm{u},j} \end{Bmatrix} \right\|^2 \\ &\text{subject to} \quad && \boldsymbol{\alpha}_{\mathrm{L}} \le \boldsymbol{\alpha} \le \boldsymbol{\alpha}_{\mathrm{U}}; \quad \boldsymbol{\beta}_{\mathrm{L}} \le \boldsymbol{\beta} \le \boldsymbol{\beta}_{\mathrm{U}}; \quad \boldsymbol{\tau}_{\mathrm{L}} \le \boldsymbol{\tau} \le \boldsymbol{\tau}_{\mathrm{U}}; \quad \boldsymbol{\eta}_{\mathrm{L}} \le \boldsymbol{\eta} \le \boldsymbol{\eta}_{\mathrm{U}} \end{aligned} \tag{17}$$

where $\|\bullet\|$ denotes any vector norm; n_{m} denotes the number of measured modes from experiments; ω_j denotes the j-th modal frequency extracted from experimental data; $\boldsymbol{\psi}_{\mathrm{m},j}$ denotes the entries in the j-th mode shape that correspond to measured (instrumented) DOFs; $\boldsymbol{\psi}_{\mathrm{u},j}$ correspond to unmeasured DOFs; The unmeasured DOFs in $\boldsymbol{\psi}_{\mathrm{u},j}$ may include these in the substructure and these representing the residual structure; therefore, not all DOFs of the substructure have to be instrumented. $\boldsymbol{\alpha}$, $\boldsymbol{\beta}$, $\boldsymbol{\tau}$ and $\boldsymbol{\eta}$ are the system parameters to be updated (see Equations (14) and (16)). Constants $\boldsymbol{\alpha}_{\mathrm{L}}$, $\boldsymbol{\beta}_{\mathrm{L}}$, $\boldsymbol{\tau}_{\mathrm{L}}$ and $\boldsymbol{\eta}_{\mathrm{L}}$ denote the lower bounds for vectors $\boldsymbol{\alpha}$, $\boldsymbol{\beta}$, $\boldsymbol{\tau}$ and $\boldsymbol{\eta}$, respectively; $\boldsymbol{\alpha}_{\mathrm{U}}$, $\boldsymbol{\beta}_{\mathrm{U}}$, $\boldsymbol{\tau}_{\mathrm{U}}$ and $\boldsymbol{\eta}_{\mathrm{U}}$ denote the upper bounds for vectors $\boldsymbol{\alpha}$, $\boldsymbol{\beta}$, $\boldsymbol{\tau}$ and $\boldsymbol{\eta}$, respectively. Note that the sign "$\leqslant$" in Equation (17) is overloaded to represent element-wise inequality.

In summary, ω_j and $\boldsymbol{\psi}_{\mathrm{m},j}$ are extracted using experimental data from the sensors deployed on the substructure and interface DOFs at high density, and thus, are constant in the optimization problem. Although ω_j and $\boldsymbol{\psi}_{\mathrm{m},j}$ are from the original structural matrices, they agree very closely to the resonance frequencies and mode shapes from the condensed structural matrices. The differences are usually negligible for the modes with lowest frequencies, i.e. these practically measurable modes. The optimization variables are $\boldsymbol{\alpha}$, $\boldsymbol{\beta}$, $\boldsymbol{\tau}$, $\boldsymbol{\eta}$ and $\boldsymbol{\psi}_{\mathrm{u}}$. Equation

(17) leads to a non-convex optimization problem that is generally difficult to solve. However, if mode shapes at unmeasured DOFs, $\boldsymbol{\psi}_{\mathrm{u}}$, were known, Equation (17) becomes a convex optimization problem. This is because given $\boldsymbol{\psi}_{\mathrm{u},j}$ is constant, the expression $\left[\tilde{\mathbf{K}}(\boldsymbol{\alpha},\boldsymbol{\tau})-\omega_j^2\tilde{\mathbf{M}}(\boldsymbol{\beta},\boldsymbol{\eta})\right]\begin{Bmatrix}\boldsymbol{\psi}_{\mathrm{m},j}\\ \boldsymbol{\psi}_{\mathrm{u},j}\end{Bmatrix}$ is an affine function on variables $\boldsymbol{\alpha}$, $\boldsymbol{\beta}$, $\boldsymbol{\tau}$ and $\boldsymbol{\eta}$. In addition, the composition of a norm function and an affine function remains convex (Berger 1990; Barvinok 2002; Boyd and Vandenberghe 2004). Therefore, the objective function in Equation (17), which is the summation of convex functions, remains convex (Boyd and Vandenberghe 2004; Zhu and Wang 2012). Besides, the lower and upper bound constraints on entries of $\boldsymbol{\alpha}$, $\boldsymbol{\beta}$, $\boldsymbol{\tau}$ and $\boldsymbol{\eta}$ provide a convex set. When minimizing a convex objective function over a convex set, the optimization problem in Equation (17) becomes convex. Likewise, if system parameters ($\boldsymbol{\alpha}$, $\boldsymbol{\beta}$, $\boldsymbol{\tau}$ and $\boldsymbol{\eta}$) were known, Equation (17) also becomes a convex optimization problem with variable $\boldsymbol{\psi}_{\mathrm{u}}$. Therefore, an iterative linearization procedure for efficiently solving the optimization problem is adopted in this study, similar to (Farhat and Hemez 1993). Figure 2 shows the pseudo code of the procedure. Each iteration step involves two operations, modal expansion and parameter updating.

```
start with α, β, τ and η = 0 (meaning M and K start with M0 and K0 );
REPEAT {
  (i)  hold α, β, τ and η as constant and minimize over variable ψu;
  (ii) hold ψu as constant and minimize over variables α, β, τ and η ;
} UNTIL convergence;
```

Figure 2. Pseudo code of the iterative linearization procedure

(i) Modal expansion

At each iteration step, operation (i) is essentially modal expansion for unmeasured DOFs, where system parameters ($\boldsymbol{\alpha}$, $\boldsymbol{\beta}$, $\boldsymbol{\tau}$ and $\boldsymbol{\eta}$) are treated as constant. At the first iteration step, these parameter values are set to be zero. At later iteration steps, the parameter values are obtained from model updating results in the previous step. When model parameters are held constant, $\boldsymbol{\psi}_{\mathrm{u}}$ becomes the only optimization variable in Equation (17). Regardless which vector norm function is adopted, the optimization problem remain convex and can be

efficiently solved using off-the-shelf solvers such as CVX (Grant and Boyd 2014). When Euclidean norm (2-norm) is adopted, the optimization problem, without constraints, is equivalent to a least square problem. The unknown part of the *j*-th experimental mode shape vector, $\boldsymbol{\psi}_{\mathrm{u},j}$, can be obtained from following least-square solution.

$$\begin{bmatrix} \mathbf{D}_{j,\mathrm{mu}} \\ \mathbf{D}_{j,\mathrm{uu}} \end{bmatrix} \boldsymbol{\psi}_{\mathrm{u},j} = -\begin{bmatrix} \mathbf{D}_{j,\mathrm{mm}} \\ \mathbf{D}_{j,\mathrm{um}} \end{bmatrix} \boldsymbol{\psi}_{\mathrm{m},j} \tag{18}$$

where definition for $\mathbf{D}_j$ comes from the generalized eigenvalue formulation.

$$\begin{bmatrix} \mathbf{D}_{j,\mathrm{mm}} & \mathbf{D}_{j,\mathrm{mu}} \\ \mathbf{D}_{j,\mathrm{um}} & \mathbf{D}_{j,\mathrm{uu}} \end{bmatrix} = \begin{bmatrix} \mathbf{D}_j \end{bmatrix} = \tilde{\mathbf{K}}(\boldsymbol{\alpha},\boldsymbol{\tau}) - \omega_j^2 \tilde{\mathbf{M}}(\boldsymbol{\beta},\boldsymbol{\eta}) \tag{19}$$

Here $\tilde{\mathbf{K}}$ and $\tilde{\mathbf{M}}$ are matrices assembled according to Equations (14) and (16). In operation (i), the matrices are constant because system parameters ($\boldsymbol{\alpha}$, $\boldsymbol{\beta}$, $\boldsymbol{\tau}$ and $\boldsymbol{\eta}$) are held constant.

(ii) Parameter updating

Operation (ii) at each iteration step is the updating of model parameters ($\boldsymbol{\alpha}$, $\boldsymbol{\beta}$, $\boldsymbol{\tau}$ and $\boldsymbol{\eta}$), using the expanded complete mode shapes. Thus, $\boldsymbol{\psi}_{\mathrm{u}}$ is held as constant in operation (ii). Again, the optimization problem with $\boldsymbol{\alpha}$, $\boldsymbol{\beta}$, $\boldsymbol{\tau}$ and $\boldsymbol{\eta}$ as optimization variables can be efficiently solved for an arbitrary vector norm function in Equation (17). When 2-norm is adopted, the problem without constraints is equivalent to a least square form shown below.

$$\begin{bmatrix} \mathbf{P}_\alpha & \mathbf{P}_\beta & \mathbf{P}_\tau & \mathbf{P}_\eta \end{bmatrix} \begin{Bmatrix} \boldsymbol{\alpha} \\ \boldsymbol{\beta} \\ \boldsymbol{\tau} \\ \boldsymbol{\eta} \end{Bmatrix} = \begin{Bmatrix} \left(\omega_1^2 \tilde{\mathbf{M}}_0 - \tilde{\mathbf{K}}_0\right) \boldsymbol{\psi}_1 \\ \vdots \\ \left(\omega_{n_\mathrm{m}}^2 \tilde{\mathbf{M}}_0 - \tilde{\mathbf{K}}_0\right) \boldsymbol{\psi}_{n_\mathrm{m}} \end{Bmatrix} \tag{20}$$

where the matrices $\mathbf{P}_\alpha$, $\mathbf{P}_\beta$, $\mathbf{P}_\tau$ and $\mathbf{P}_\eta$ are formulated as

$$\mathbf{P}_\alpha = \begin{bmatrix} \mathbf{S}_{\alpha,1}\boldsymbol{\psi}_1 & \cdots & \mathbf{S}_{\alpha,n_\alpha}\boldsymbol{\psi}_1 \\ \mathbf{S}_{\alpha,1}\boldsymbol{\psi}_2 & \cdots & \mathbf{S}_{\alpha,n_\alpha}\boldsymbol{\psi}_2 \\ \vdots & \vdots & \vdots \\ \mathbf{S}_{\alpha,1}\boldsymbol{\psi}_{n_m} & \cdots & \mathbf{S}_{\alpha,n_\alpha}\boldsymbol{\psi}_{n_m} \end{bmatrix} \qquad \mathbf{P}_\beta = \begin{bmatrix} -\omega_1^2\mathbf{S}_{\beta,1}\boldsymbol{\psi}_1 & \cdots & -\omega_1^2\mathbf{S}_{\beta,n_\beta}\boldsymbol{\psi}_1 \\ -\omega_2^2\mathbf{S}_{\beta,1}\boldsymbol{\psi}_2 & \cdots & -\omega_2^2\mathbf{S}_{\beta,n_\beta}\boldsymbol{\psi}_2 \\ \vdots & \vdots & \vdots \\ -\omega_{n_m}^2\mathbf{S}_{\beta,1}\boldsymbol{\psi}_{n_m} & \cdots & -\omega_{n_m}^2\mathbf{S}_{\beta,n_\beta}\boldsymbol{\psi}_{n_m} \end{bmatrix} \tag{21a}$$

$$\mathbf{P}_{\tau}=\begin{bmatrix}\mathbf{S}_{\tau,1}\boldsymbol{\psi}_1 & \cdots & \mathbf{S}_{\tau,n_i+n_q}\boldsymbol{\psi}_1\\ \mathbf{S}_{\tau,1}\boldsymbol{\psi}_2 & \cdots & \mathbf{S}_{\tau,n_i+n_q}\boldsymbol{\psi}_2\\ \vdots & \vdots & \vdots\\ \mathbf{S}_{\tau,1}\boldsymbol{\psi}_{n_m} & \cdots & \mathbf{S}_{\tau,n_i+n_q}\boldsymbol{\psi}_{n_m}\end{bmatrix} \qquad \mathbf{P}_{\eta}=\begin{bmatrix}-\omega_1^2\mathbf{S}_{\eta,1}\boldsymbol{\psi}_1 & \cdots & -\omega_1^2\mathbf{S}_{\eta,n_i+n_q}\boldsymbol{\psi}_1\\ -\omega_2^2\mathbf{S}_{\eta,1}\boldsymbol{\psi}_2 & \cdots & -\omega_2^2\mathbf{S}_{\eta,n_i+n_q}\boldsymbol{\psi}_2\\ \vdots & \vdots & \vdots\\ -\omega_{n_m}^2\mathbf{S}_{\eta,1}\boldsymbol{\psi}_{n_m} & \cdots & -\omega_{n_m}^2\mathbf{S}_{\eta,n_i+n_q}\boldsymbol{\psi}_{n_m}\end{bmatrix} \tag{21b}$$

Here $\mathbf{S}_{\alpha,j}$, $\mathbf{S}_{\beta,j}$, $\mathbf{S}_{\tau,j}$ and $\mathbf{S}_{\eta,j}$ represent the constant sensitivity matrices from Equations (14) and (16); $\boldsymbol{\psi}_j$ is the *j*-th expanded mode containing both measured and unmeasured DOFs.

As stated in the beginning of this section, Equation (17) leads to a non-convex optimization problem. Therefore, in general, no algorithm guarantees to find the exact global optimum (Berger 1990; Barvinok 2002; Boyd and Vandenberghe 2004). Although the performance of the iterative linearization procedure appears to be acceptable, future research is needed to identify the mathematical conditions that render a solution close to the global optimum

Modal Property Difference Approach

For comparison, substructure model updating is also performed through a widely used conventional approach that minimizes experimental and simulated modal property differences (Link 1998). The conventional model updating formulation aims to minimize the difference between experimental and simulated natural frequencies, as well as the difference between experimental and simulated mode shapes of the substructure.

$$\underset{\boldsymbol{\alpha},\boldsymbol{\beta},\boldsymbol{\tau},\boldsymbol{\eta}}{\text{minimize}} \quad \sum_{j=1}^{n_m}\left\{\left(\frac{\omega_j^{\text{FE}}-\omega_j}{\omega_j}\right)^2+\left(\frac{1-\sqrt{\text{MAC}_j}}{\sqrt{\text{MAC}_j}}\right)^2\right\} \tag{22}$$

where ω_j^{FE} and ω_j represent the *j*-th simulated (from the condensed model in Equations (14) and (16)) and experimentally extracted frequencies, respectively; MAC_j represents the modal assurance criterion evaluating the difference between the *j*-th simulated and experimental mode shapes. Note that only mode shape entries corresponding to measured DOFs are compared (i.e. between $\boldsymbol{\psi}_{\text{m},j}^{\text{FE}}$ and $\boldsymbol{\psi}_{\text{m},j}$). The optimization variables are $\boldsymbol{\alpha}$, $\boldsymbol{\beta}$, $\boldsymbol{\tau}$, $\boldsymbol{\eta}$. The mode shapes at unmeasured DOFs, $\boldsymbol{\psi}_{\text{u},j}$, are not among the optimization variables for modal

property difference approach, because MAC_j only compares the mode shapes at measured DOFs. A nonlinear least-square optimization solver, `'lsqnonlin'` in MATLAB optimization toolbox (MathWorks Inc. 2011), is adopted to numerically solve the optimization problem minimizing modal property differences. The optimization solver seeks a minimum through Levenberg-Marquardt algorithm, which adopts a search direction interpolated between the Gauss-Newton direction and the steepest descent direction (Moré 1978).

It should be noted that if all the stiffness and mass parameters in the substructure are updated simultaneously, neither the modal dynamic residual approach nor the modal property difference approach has a unique solution for the stiffness and mass parameters. The reason is that arbitrary scaling to the generalized eigenvalue equation (involving mass and stiffness matrices) does not affect the standing of the equation. In other words, the matrix pair **K** and **M** have the same generalized eigenvalue solutions as 2**K** and 2**M**. Therefore, some parameters (which oftentimes are mass parameters in which one has higher confidence) for at least part of the substructure should be regarded as constant and cannot be updated.

NUMERICAL VALIDATION

To validate the proposed modal dynamic residual approach for substructure model updating, numerical simulations are conducted. In each simulation example, the modal dynamic residual approach and modal property difference approach are compared. For each approach, the updating is performed assuming only a few measured modes corresponding to the few lowest natural frequencies are available, as happens in practice. The first subsection describes substructure model updating on a lumped spring-mass model. The second subsection describes a plane truss model. The last subsection describes a space frame model.

Lumped Spring-Mass Model

Figure 3 shows a 200-DOF lumped spring-mass model for validating the proposed substructure updating approach. In the initial model (as starting point of model updating), all the mass and spring stiffness values are set identically as 6kg and 35kN/m, respectively. To construct the actual model (as updating goal), damage is

introduced to this model by reducing 10% of spring stiffness at k_{20}, k_{30}, k_{45}, k_{50}, k_{60}, k_{62}, k_{82}, k_{100}, k_{120}, and k_{150}. A substructure with DOFs from 41 to 54 ($\mathbf{x}_S \in \mathbb{R}^{14\times1}$) is selected for model updating. As a result, DOFs 40 and 55 are interface DOFs ($\mathbf{x}_I \in \mathbb{R}^{2\times1}$). All other DOFs belong to the residual structure. The initial stiffness, actual stiffness, and expected model updating changes in the substructure are listed in TABLE 1. Note that two springs with stiffness loss, k_{45} and k_{50}, are contained in the substructure, but most other stiffness losses occur in the residual structure. It is assumed all substructure and interface DOFs are instrumented with sensors for experimentally capturing substructure vibration modes. No measurement is required on the residual structure.

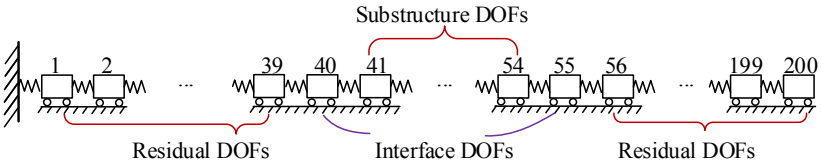

Figure 3. Illustration of substructure selection; for the actual structure model (to be identified), 10% stiffness reduction is introduced to k_{20}, k_{30}, k_{45}, k_{50}, k_{60}, k_{62}, k_{82}, k_{100}, k_{120}, and k_{150} as damage

TABLE 1. Structural properties in the selected substructure

Updating parameter	k_{41}	k_{42}	k_{43}	k_{44}	k_{45}	k_{46}	k_{47}	k_{48}	k_{49}	k_{50}	k_{51}	k_{52}	k_{53}	k_{54}	k_{55}
Initial value (kN/m)	35	35	35	35	35	35	35	35	35	35	35	35	35	35	35
Actual value (kN/m)	35	35	35	35	31.5	35	35	35	35	31.5	35	35	35	35	35
Change (%)	0	0	0	0	-10	0	0	0	0	-10	0	0	0	0	0

When formulating model condensation, dynamic response of the residual structure is approximated using twenty modal coordinates, i.e. $n_q = 20$ (Equation (3)). With $\mathbf{x}_S \in \mathbb{R}^{14\times1}$ and $\mathbf{x}_I \in \mathbb{R}^{2\times1}$, the entire structural model is therefore condensed to 36 DOFs. Without loss of generality, accurate structural mass matrix is assumed to be known; therefore mass parameters $\boldsymbol{\beta}$ (Equation (16)) is not among the updating parameters. The updating variables are the stiffness parameters $\boldsymbol{\alpha}$ (corresponding to relative changes ratio of k_{41}, k_{42}, ..., and k_{55} in the substructure), and modal parameters of the residual structural with free interface (τ_2, τ_3, ..., τ_{22} and η_1, η_2, ..., η_{22}). Note that $n_I + n_q = 22$ and that the modal parameter τ_1 is not included, because the first resonance frequency of the residual structure with free interface is zero (corresponding to free-body movement). As a

result, the first modal correction matrix $\tilde{\mathbf{K}}_{\mathrm{R}0,1}$ in Equation (14) is a zero matrix, and so is the corresponding sensitivity matrix $\mathbf{S}_{\tau,1}$. Using modal frequencies and substructure mode shapes of the actual structure with reduced stiffness (ω_j and $\boldsymbol{\psi}_{\mathrm{m},j}$) as "experimental data", both the proposed modal dynamic residual approach and the conventional modal property difference approach are applied.

TABLE 2 summarizes the updating results using the proposed modal dynamic residual approach for substructure model updating. With different numbers of measured modes available, ranging from three to six lowest natural frequencies, the updated values for k_{45} and k_{50} are exactly -10.0% and -10.0%. The updated values for all other k_i are exactly zero, which implies no change in all other stiffness values in the substructure. Therefore, the updating of substructure parameters achieve the goal (shown in TABLE 1) and correctly identify the stiffness loss locations and degrees of stiffness loss. Figure 4 plots the relative errors of the updating results, i.e. deviation of updated stiffness values from the actual values, for different numbers of available modes. The figure also shows that the updating results accurately identify all substructure stiffness parameters, because all the updating errors are less than 0.0005%.

TABLE 2. Updated parameter changes (%) for substructure elements on the lumped spring-mass model by minimization of modal dynamic residuals

Available modes	k_{41}	k_{42}	k_{43}	k_{44}	k_{45}	k_{46}	k_{47}	k_{48}	k_{49}	k_{50}	k_{51}	k_{52}	k_{53}	k_{54}	k_{55}
3 modes	0.00	0.00	0.00	0.00	-10.00	0.00	0.00	0.00	0.00	-10.00	0.00	0.00	0.00	0.00	0.00
4 modes	0.00	0.00	0.00	0.00	-10.00	0.00	0.00	0.00	0.00	-10.00	0.00	0.00	0.00	0.00	0.00
5 modes	0.00	0.00	0.00	0.00	-10.00	0.00	0.00	0.00	0.00	-10.00	0.00	0.00	0.00	0.00	0.00
6 modes	0.00	0.00	0.00	0.00	-10.00	0.00	0.00	0.00	0.00	-10.00	0.00	0.00	0.00	0.00	0.00

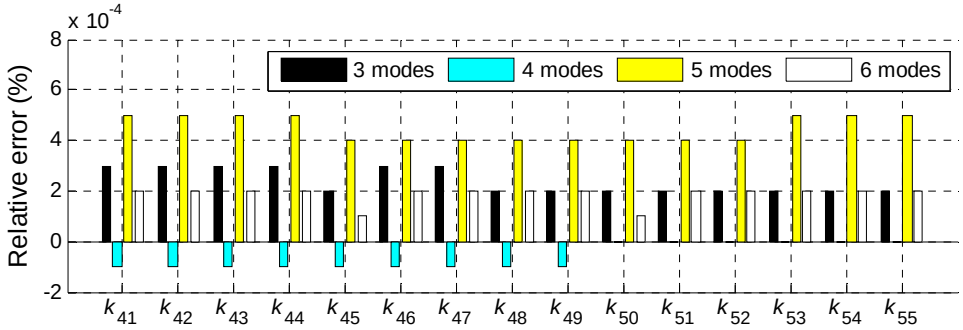

Figure 4. Relative errors of the updated parameters on the lumped spring-mass model by minimization of modal dynamic residuals

Similarly, TABLE 3 summarizes the updating results using the conventional modal property difference approach (Equation (22)). The overall model updating performance is obviously worse than the modal dynamic residual approach. Figure 5 shows the relative errors of the updating results, as compared to the actual values. The maximum relative error for conventional modal property difference approach is 3.3% for parameter k_{45} (with three measured modes available). Therefore, the conventional approach shows worse performance than the proposed modal dynamic residual approach.

TABLE 3. Updated parameter changes (%) for substructure elements on the lumped spring-mass model by minimization of modal property differences

Available modes	k_{41}	k_{42}	k_{43}	k_{44}	k_{45}	k_{46}	k_{47}	k_{48}	k_{49}	k_{50}	k_{51}	k_{52}	k_{53}	k_{54}	k_{55}
3 modes	-0.10	0.03	-0.37	-1.93	-6.69	-1.84	-0.30	-0.28	-1.82	-6.83	-1.91	-0.33	0.09	0.09	-0.15
4 modes	0.25	0.32	0.37	-0.16	-9.50	-0.11	0.31	0.26	0.02	-9.73	0.05	0.23	0.14	0.17	0.14
5 modes	0.57	0.91	0.76	-0.64	-7.89	-0.56	0.89	0.88	-0.62	-7.70	-0.70	0.78	1.04	0.95	0.07
6 modes	0.61	1.32	1.35	1.33	-8.77	1.37	1.42	1.44	1.44	-8.66	1.47	1.54	1.50	1.54	1.73

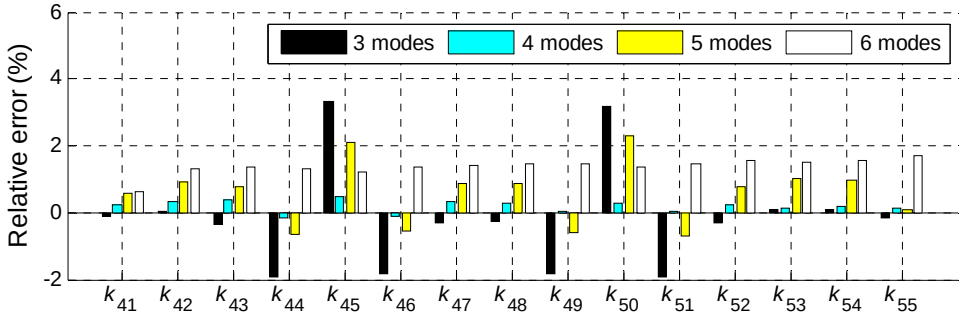

Figure 5. Relative errors of the updated parameters on the lumped spring-mass model by minimization of modal property differences

Plane Truss Model

Figure 6 shows the plane truss model for validating the proposed substructure updating approach. The truss model has 26 nodes, and each node has two translational DOFs. Horizontal and vertical springs (k_{x1} and k_{y1}) are allocated at the left support to simulate a non-ideal hinge, while a vertical spring (k_{y2}) is allocated at the right support to simulate a non-ideal roller. TABLE 4 summarizes the structural properties of the model, including elastic modulus E_1 of top-level truss bars, modulus E_2 of diagonal and vertical bars, modulus E_3 of

bottom bars, and three spring stiffness numbers. The table provides initial nominal values for all parameters, as starting point for model updating. The table also lists actual values, which ideally are to be identified. The relative changes from initial to actual values are also listed.

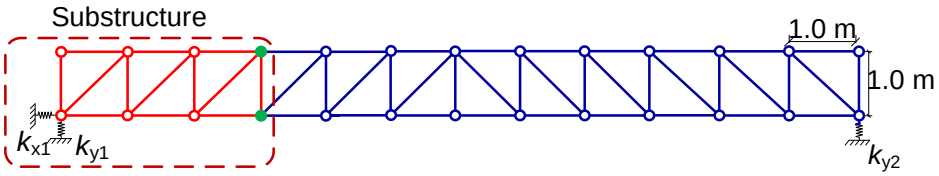

Figure 6. Illustration of substructure selection of a plane truss

TABLE 4. Structural properties of the plane truss

Updating parameter	Steel elastic modulus (10^{11} N/m^2)			k_{x1} (10^6 N/m)	k_{y1} (10^6 N/m)	k_{y2} (10^6 N/m)
	Top (E_1)	Diag. & Vert. (E_2)	Bottom (E_3)			
Initial value	2	2	2	5	5	5
Actual value	2.2	2.1	1.9	2	7	7
Change (%)	10	5	-5	-60	40	40

A substructure containing first three truss units from left is selected for model updating (Figure 6). The selected substructure contains six substructure nodes and two interface nodes. Each node includes two translational DOFs. The substructure DOF vector is $\mathbf{x}_S \in \mathbb{R}^{12\times1}$ and the interface DOF vector is $\mathbf{x}_I \in \mathbb{R}^{4\times1}$. It is assumed all substructure and interface DOFs are instrumented with sensors for experimentally capturing substructure vibration modes. No measurement is required on the residual structure. For modeling, dynamic response of the residual structure is approximated using ten modal coordinates, i.e. $n_q = 10$ in Equation (3). As a result, the entire structural model is condensed to $n_S + n_I + n_q = 26$ DOFs (from 52 DOFs in the original structure). The substructure stiffness parameters (to be updated) include the three elastic moduli in the substructure (E_1, E_2, and E_3), as well as the spring stiffness values at the left support (k_{x1} and k_{y1}). Because the spring stiffness at the right support, k_{y2}, only contributes to residual structure, k_{y2} cannot be updated. Instead, the residual structure is updated through modal parameters of the residual structure with free interface (τ_2, τ_3, ..., τ_{14} and η_1, η_2, ..., η_{14}).

Note that $n_1 + n_q = 14$ and that the modal parameters τ_1 is not included, because the first resonance frequency of the residual structure with free interface is zero, similar as the lumped spring-mass model in the last subsection.

TABLE 5 summarizes the updating results using the proposed modal dynamic residual approach for substructure model updating. The results are presented in terms of relative change percentages from initial values. For every available number of modes, the updating parameter changes are close to the ideal percentages listed in TABLE 4. Figure 7 plots the relative errors of the updating results, i.e. deviation of updated stiffness values from the actual values, for different numbers of available modes. The figure shows that the updating results accurately identify all substructure properties, and the maximum updating error is a negligible 0.08% for parameter E_1 (when only three modes are available).

TABLE 5. Updated parameter changes (%) for substructure elements on the plane truss model by minimization of modal dynamic residuals

Available modes	Steel elastic modulus change (%)			Change in k_{x1} (%)	Change in k_{y1} (%)
	Top (E_1)	Diag. & Vert. (E_2)	Bottom (E_3)		
3 modes	10.08	5.03	-5.02	-60.00	40.04
4 modes	9.99	5.00	-5.00	-60.00	40.00
5 modes	9.99	4.99	-4.98	-60.00	39.99
6 modes	10.04	4.99	-4.98	-60.00	39.99

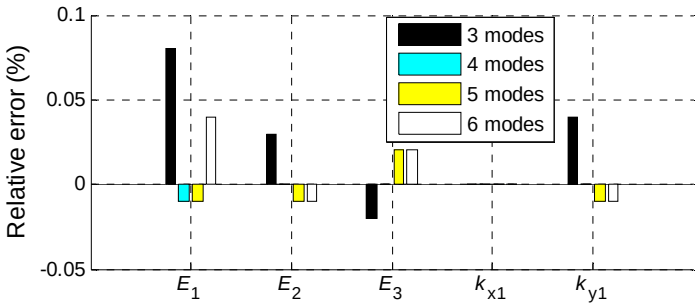

Figure 7. Relative errors of the updated parameters on the plane truss model by minimization of modal dynamic residuals

Similarly, TABLE 6 summarizes the updating results using the conventional modal property difference approach. The updated parameter changes are apparently different from the ideal percentages listed in TABLE 4. Figure 8 shows the relative errors of the updating results, as compared to the actual values. The conventional

approach can update some structural properties to a fairly good accuracy, but the results are generally worse than the proposed modal dynamic residual approach. The maximum error for conventional modal property difference approach is -7.98% for parameter E_1 (with five available modes).

TABLE 6. Updated parameter changes (%) for substructure elements on the plane truss model by minimization of modal property differences

Available modes	Steel elastic modulus change (%)			Change in k_{x1} (%)	Change in k_{y1} (%)
	Top (E_1)	Diag. & Vert. (E_2)	Bottom (E_3)		
3 modes	5.23	2.84	-7.86	-60.2	37.02
4 modes	7.71	4.59	-4.58	-58.44	38.90
5 modes	2.03	7.70	-5.88	-57.82	38.23
6 modes	4.33	7.74	0.16	-55.43	41.11

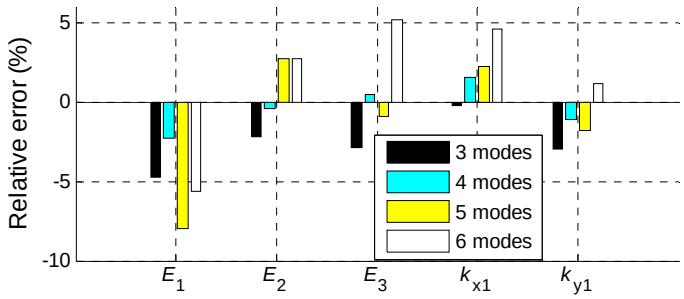

Figure 8. Relative errors of the updated parameters on the plane truss model by minimization of modal property differences

Space Frame Model

Figure 9 shows the simulation model of a space frame bridge. The space frame model contains 46 nodes, each node with six spatial DOFs. Although mainly a frame structure, the segment cross bracings in top plane and two side planes are truss members. Transverse and vertical springs (k_y and k_z) are allocated at both ends of the frame structure to simulate non-ideal boundary conditions. TABLE 7 summarizes the structural stiffness parameters of the model. The parameters are divided into three categories. The first category contains six parameters (starting from top in the table), which are elastic moduli of the frame and truss (diagonal bracings in top plane) members along the entire length of the frame structure. The second category contains ten parameters, which are the elastic moduli of truss members (diagonal bracings in two side planes) for different

segments. The third category contains stiffness parameters of the four types of support springs. TABLE 7 provides initial (nominal) values for all parameters, as starting point for model updating. The table also lists actual values, which ideally are to be identified. Note that for demonstration, some actual values are larger than initial values, while others are smaller. The relative changes from initial to actual values, to be identified, are also listed.

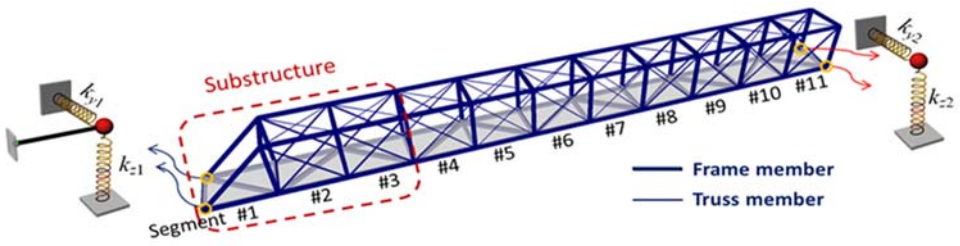

Figure 9. Illustration of substructure selection of a space frame bridge

TABLE 7. Structure stiffness parameters

Updating parameters			Initial value	Actual value	Change (%)
Elastic moduli of members along the frame structure (kips/in^2)	Frame members	E_1 – Longitudinal top chord	29,000	30,450	5
		E_2 – Longitudinal bottom chord	29,000	30,450	5
		E_3 – Vertical members	29,000	27,550	-5
		E_4 – Transverse top chord	29,000	26,100	-10
		E_5 – Transverse & diagonal bottom chord	29,000	30,450	5
	Truss members	E_6 – Diagonal bracings in top plane	29,000	27,550	-5
Elastic moduli of side-plane diagonal bracings (truss members) for each segment (kips/in^2)	E_{S2} – 2nd segment		29,000	26,100	-10
	E_{S3} – 3rd segment		29,000	26,100	-10
	E_{S4} – 4th segment		29,000	26,100	-10
	E_{S5} – 5th segment		29,000	27,550	-5
	E_{S6} – 6th segment		29,000	27,550	-5
	E_{S7} – 7th segment		29,000	27,550	-5
	E_{S8} – 8th segment		29,000	24,650	-15
	E_{S9} – 9th segment		29,000	26,100	-10
	E_{S10} – 10th segment		29,000	27,550	-5
	E_{S11} – 11th segment		29,000	27,550	-5
Support springs (kips/in)	k_{y1} – Left transverse		200	140	-30
	k_{z1} – Left vertical		500	800	60
	k_{y2} – Right transverse		200	140	-30
	k_{z2} – Right vertical		500	800	60

A substructure containing first three segments from left is selected for model updating (Figure 9). The selected substructure contains 10 substructure nodes and 4 interface nodes. Since each node has six DOFs and the longitudinal DOFs of the two support nodes are constrained, the substructure DOF vector is $\mathbf{x}_S \in \mathbb{R}^{58\times1}$ and the interface DOF vector is $\mathbf{x}_I \in \mathbb{R}^{24\times1}$. For practicality, it is assumed only translational DOFs of the substructure and interface nodes are instrumented with accelerometers for capturing substructure vibration modes; rotational DOFs are not measured. No measurement is required on the residual structure. For model condensation, dynamic response of the residual structure is approximated using twenty modal coordinates, i.e. n_q = 20 in Equation (3). As a result, the entire structural model is condensed to $n_S + n_I + n_q$ = 102 DOFs (reduced from 274 DOFs in the original structure).

Figure 10 shows the detailed view of the substructure containing the first three segments. The substructure stiffness parameters (to be updated) include the five elastic moduli of the frame members (E_1~E_5), the elastic moduli of top bracing truss members (E_6), the elastic moduli of side-bracing truss members at the 2nd and 3rd segments (E_{S2} and E_{S3}), and the spring stiffness values at the left support (k_{y1} and k_{z1}). On the other hand, the residual structure is updated through modal parameters of the residual structure with free interface (τ_2, τ_3, ..., τ_{44} and η_1, η_2, ..., η_{44}). Note that $n_I + n_q = 44$ and that modal parameter τ_1 is not included, similar as previous examples.

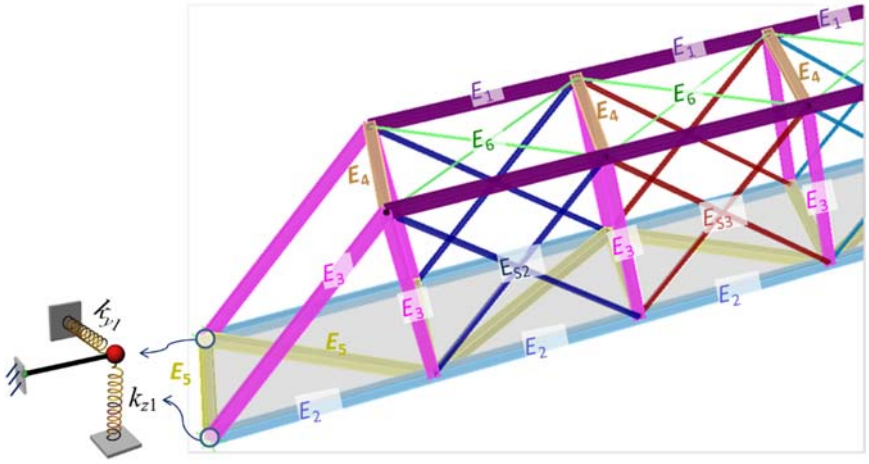

Figure 10. Detailed view of the substructure showing stiffness parameters to be updated

TABLE 8 summarizes the updating results using the proposed modal dynamic residual approach for substructure model updating. The results are presented in terms of relative change percentages from initial values. For every available number of modes, most of the updated parameter changes are close to the ideal percentages listed in TABLE **7**. The updating results for E_4, the elastic moduli of the transverse frame members in top plane, are between -5.90% (with 5 modes) and -5.48% (with four available modes). These results are most different from the actual/ideal change of -10%. The reason is this parameter is less sensitive to translational DOFs, which can be explained by a sensitivity analysis performed to each stiffness parameter perturbed around the initial parameter values. Due to page limit, Figure 11 shows the sensitivity plots of two updating parameters, E_4 and E_6. The objective function (Equation (17)) is calculated by changing the selected parameter from -20% to +20%, while keeping all other parameters at initial values. The plots show that the objective function varies within a smaller range (8825~8835) for E_4, while within a much larger range (8782~8924) for E_6. The comparison demonstrates that E_4 is not a sensitive updating parameter. Figure 12 plots the relative errors of the updating results, i.e. relative difference of updated values from the actual parameter values, for different numbers of available modes. The figure shows that except for E_4, the updating results accurately identify all other substructure stiffness parameters. In addition, the updating accuracy generally improves when more measured modes are available.

TABLE 8. Updated parameter changes (%) for substructure elements on the space frame model by minimization of modal dynamic residuals

Available modes	Frame member					Truss member			Spring	
	E_1	E_2	E_3	E_4	E_5	E_6	E_{S2}	E_{S3}	k_{y1}	k_{z1}
3 modes	4.21	4.17	-5.61	-5.76	4.16	-6.24	-10.68	-10.94	-30.54	59.01
4 modes	4.70	4.65	-5.08	-5.48	4.64	-5.61	-10.26	-10.61	-30.21	59.90
5 modes	4.91	5.00	-5.05	-5.90	4.99	-5.16	-10.05	-10.48	-29.99	59.94
6 modes	4.73	4.39	-5.10	-5.65	4.36	-6.39	-10.32	-12.11	-30.43	59.83

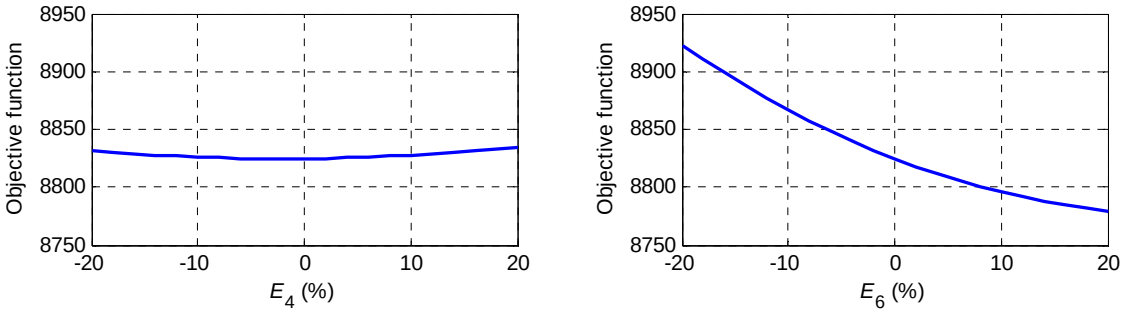

Figure 11. Sensitivities of the updated parameters to the objective function

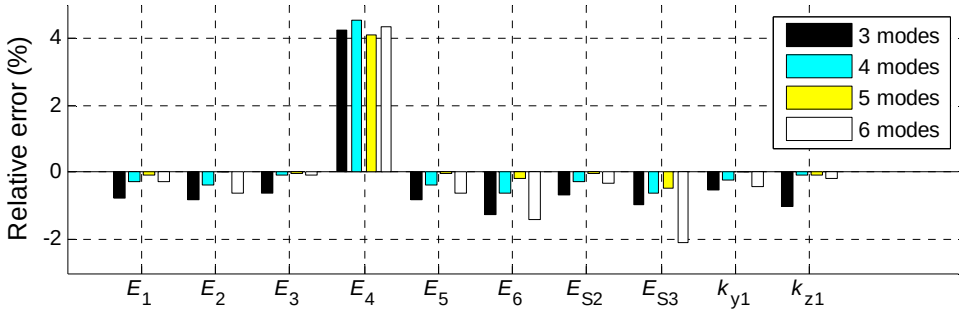

Figure 12. Relative errors of the updated parameters on the space frame model by minimization of modal dynamic residuals

TABLE 9 summarizes the updating results using the conventional approach minimizing modal property differences. Many of the updated/identified parameter changes are apparently different from the correct/ideal values listed in TABLE 7. Figure 13 plots the relative errors of the updating results. The figure shows that the updating results from conventional approach have much larger errors than the results from the proposed modal dynamic residual approach (Figure 12), particularly for stiffness parameters k_{y1} and k_{z1} of the support spring. The conventional approach minimizing modal property differences, when used for substructure model updating, cannot achieve a reasonable accuracy in this example.

TABLE 9. Updated parameter changes (%) for substructure elements on the space frame model by minimization of modal property differences

Available modes	Frame member					Truss member			Spring	
	E_1	E_2	E_3	E_4	E_5	E_6	E_{S2}	E_{S3}	k_{y1}	k_{z1}
3 modes	3.21	5.89	-4.68	-2.40	1.77	-4.25	-3.12	-2.74	0.02	0.00
4 modes	3.60	5.18	-5.71	-3.53	1.64	-5.60	-3.06	-2.97	0.02	0.02
5 modes	4.78	6.83	-5.01	-4.87	3.73	-2.49	-1.49	-1.21	0.05	0.06
6 modes	6.93	6.42	-5.58	-8.25	3.53	-4.69	-2.84	-2.72	-0.22	0.13

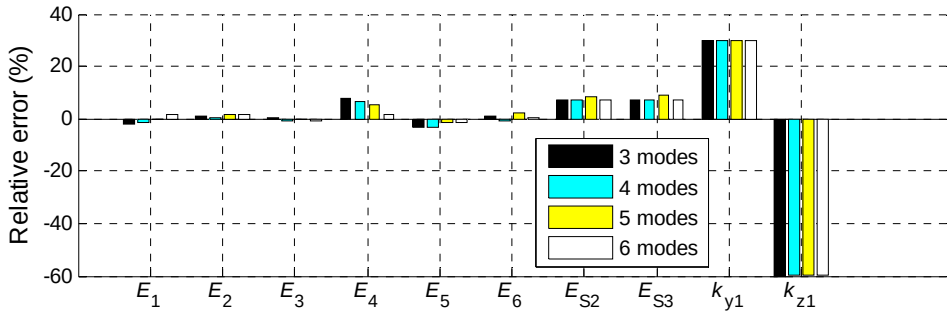

Figure 13. Relative errors of the updated parameters on the space frame model by minimization of modal property differences

Discussion of Model Updating Results

The numerical simulations in this section demonstrate that the proposed substructure updating approach minimizing modal dynamic residuals is capable of accurately identifying most parameters in the substructure. Meanwhile, when the conventional approach minimizing modal property differences is applied, the updating process either generates results with much lower accuracy (spring-mass and plane truss models), or cannot achieve a reasonable solution at all for some parameters (space frame model). The main reason is likely that the objective function in the modal property difference approach is less sensitive to minor changes in structural parameters. In addition, according to the numerical examples studied thus far, more measured modes usually help enable more accurate updating results. However, the mathematical conditions that render a solution close to the global optimum, or formulas that can gage the proximity to the global optimum (without knowing the solution in advance) would require much future research.

It should be noted that the solutions given by the proposed modal dynamic residual approach still show small errors. The errors are mainly caused by the approximations made in the model condensation process for substructure model updating. First, the Craig-Bampton transform used in model condensation adopts the static condensation matrix as the transformation matrix from interface DOFs to residual DOFs (Equation (3)), which neglects interface dynamic contribution. Second, the Craig-Bampton transform uses only a few dominant modes describing dynamic behavior of the residual structure; higher-frequency modes are neglected. Third,

while updating modal parameters for the residual structure, it is assumed that potential physical parameter changes in the residual structure do not significantly alter the generalized eigenvectors of the residual structural matrices (Equation (11)). Nevertheless, the overall substructure updating performance through minimization of modal dynamic residuals is reasonably accurate.

CONCLUSIONS AND FINDINGS

This paper studies an iterative linearization procedure for substructure model updating, where the entire structural model is divided into the substructure (currently being instrumented and to be updated) and the residual structure. Physical parameters in the substructure and modal parameters of the residual structure are chosen as optimization variables; minimization of the modal dynamic residuals is adopted as the optimization objective. Following conclusions and findings are made from this research:

- To make substructure model updating more feasible, Craig-Bampton transform is an effective method that can condense the residual structure using a limited number of dominant mode shapes, while the substructure model remains at high resolution.
- Numerical studies demonstrate that the combination of Craig-Bampton transform and modal dynamic residual approach can successfully update the physical parameters in the substructure with acceptable accuracy.
- Validated by 1D, 2D and 3D examples, the iterative linearization procedure proves effective in finding a solution to the optimization problem minimizing modal dynamic residuals.

ACKNOWLEDGEMENT

This research was partially funded by the National Science Foundation (CMMI-1150700 and CMMI-1041607) and the Georgia Department of Transportation (RP12-21). Any opinions, findings, and conclusions expressed in this publication are those of the authors and do not necessarily reflect the view of the sponsors.

REFERENCES

Barvinok, A. (2002). *A course in convexity*, American Mathematical Society Providence.

Berger, M. (1990). "Convexity." *American Mathematical Monthly*, 97(8), 650-78.

Boyd, S. P., and Vandenberghe, L. (2004). *Convex Optimization*, Cambridge University Press, Cambridge, UK ; New York.

Craig, R. R., Jr. (2000). "Coupling of substructures for dynamic analyses - an overview." Proceedings of the 41st AIAA/ASME/ASCE/AHS/ASC Structures, Structural Dynamics, and Materials Conference and Exhibit, Atlanta, GA.

Craig, R. R., Jr., and Bampton, M. C. C. (1968). "Coupling of substructures of dynamics analyses." *AIAA Journal*, 6(7), 1313-1319.

Farhat, C., and Hemez, F. M. (1993). "Updating finite element dynamic models using an element-by-element sensitivity methodology." *AIAA Journal*, 31(9), 1702-1711.

Friswell, M. I., and Mottershead, J. E. (1995). *Finite element model updating in structural dynamics*, Kluwer Academic Publishers, Dordrecht; Boston.

Grant, M., and Boyd, S. (2014). "CVX: MATLAB software for disciplined convex programming, version 2.0."

Hoshiya, M., and Saito, E. (1984). "Structural identification by extended kalman filter." *Journal of Engineering Mechanics*, 110(12), 1757-1770.

Hou, J., Jankowski, Ł., and Ou, J. (2011). "A substructure isolation method for local structural health monitoring." *Structural Control and Health Monitoring*, 18(6), 601-618.

Jaishi, B., and Ren, W. X. (2006). "Damage detection by finite element model updating using modal flexibility residual." *Journal of Sound and Vibration*, 290(1-2), 369-387.

Koh, C., and Shankar, K. (2003). "Substructural Identification Method without Interface Measurement." *Journal of Engineering Mechanics*, 129(7), 769-776.

Koh, C. G., Hong, B., and Liaw, C. Y. (2003). "Substructural and progressive structural identification methods." *Engineering Structures*, 25(12), 1551-1563.

Koh, C. G., See, L. M., and Balendra, T. (1991). "Estimation of structural parameters in time domain - a substructure approach." *Earthquake Engineering & Structural Dynamics*, 20(8), 787-801.

Link, M. (1998). "Updating analytical models by using local and global parameters and relaxed optimisation requirements." *Mechanical Systems and Signal Processing*, 12(1), 7-22.

Loh, C. H., and Tou, I. C. (1995). "A system identification approach to the detection of changes in both linear and non-linear structural parameters." *Earthquake Engineering & Structural Dynamics*, 24(1), 85-97.

MathWorks Inc. (2011). *Optimization Toolbox™ User's Guide*, Natick, MA.

Moré, J. (1978). "The Levenberg-Marquardt algorithm: Implementation and theory." Numerical Analysis, 105-116.

Sanayei, M., Arya, B., Santini, E. M., and Wadia-Fascetti, S. (2001). "Significance of Modeling Error in Structural Parameter Estimation." *Computer-Aided Civil and Infrastructure Engineering*, 16(1), 12-27.

Sanayei, M., McClain, J. A. S., Wadia-Fascetti, S., and Santini, E. M. (1999). "Parameter Estimation Incorporating Modal Data and Boundary Conditions." *Journal of Structural Engineering*, 125(9), 1048-1055.

Smyth, A. W., Masri, S. F., Chassiakos, A. G., and Caughey, T. K. (1999). "On-line parametric identification of MDOF nonlinear hysteretic systems." *Journal of Engineering Mechanics*, 125(2), 133-142.

Smyth, A. W., Masri, S. F., Kosmatopoulos, E. B., Chassiakos, A. G., and Caughey, T. K. (2002). "Development of adaptive modeling techniques for non-linear hysteretic systems." *International Journal of Non-Linear Mechanics*, 37(8), 1435-1451.

Trinh, T. N., and Koh, C. G. (2012). "An improved substructural identification strategy for large structural systems." *Structural Control and Health Monitoring*, 19(8), 686-700.

Yang, J. N., and Huang, H. (2007a). "Sequential non-linear least-square estimation for damage identification of structures with unknown inputs and unknown outputs." *International Journal of Non-Linear Mechanics*, 42(5), 789-801.

Yang, J. N., and Huang, H. (2007b). "Substructure damage identification using damage tracking technique." Proceedings of SPIE, Sensors and Smart Structures Technologies for Civil, Mechanical, and Aerospace Systems, T. Masayoshi, Y. Chung-Bang, and G. Victor, eds., SPIE, San Diego, CA, USA.

Yang, J. N., Pan, S., and Huang, H. (2007). "An adaptive extended Kalman filter for structural damage identifications II: unknown inputs." *Structural Control and Health Monitoring*, 14(3), 497-521.

Yuen, K.-V., and Katafygiotis, L. S. (2006). "Substructure identification and health monitoring using noisy response measurements only." *Computer-Aided Civil and Infrastructure Engineering*, 21(4), 280-291.

Zhang, D., and Johnson, E. A. (2013a). "Substructure identification for shear structures I: Substructure identification method." *Structural Control and Health Monitoring*, 20(5), 804-820.

Zhang, D., and Johnson, E. A. (2013b). "Substructure identification for shear structures II: Controlled substructure identification." *Structural Control and Health Monitoring*, 20(5), 821-834.

Zhao, Q., Sawada, T., Hirao, K., and Nariyuki, Y. (1995). "Localized identification of MDOF structures in the frequency domain." *Earthquake Engineering & Structural Dynamics*, 24(3), 325-338.

Zhu, D., Dong, X., and Wang, Y. (2013). "Substructure model updating through modal dynamic residual approach." Proceedings of the 9th International Workshop on Structural Health Monitoring (IWSHM), Stanford, CA - USA.

Zhu, D., and Wang, Y. (2012). "Substructure model updating through iterative convex optimization." Proceeding of the ASME 2012 Conference on Smart Materials, Adaptive Structures and Intelligent Systems (SMASIS), Stone Mountain, GA, USA, 601-607.